 doi:10.20944/preprints202208.0099.v1

Article

Enhancing Imagistic Interstitial Lung Disease Diagnosis by Using Complex Networks

Ana Adriana Trușculescu [1,4], Diana Luminița Manolescu [2,4*], Laura Broască [3], Versavia Maria Ancușa [3], Horia Ciocârlie[3], Camelia Corina Pescaru[1,4], Emanuela Vaștag[1,4] and Cristian Iulian Oancea [1,4]

1 Pulmonology Department, 'Victor Babes' University of Medicine and Pharmacy, Eftimie Murgu Square 2, 300041 Timișoara, Romania; ana.trusculescu@umft.ro(A.A.T.); pescaru.camelia@umft.ro(C.C.P.); emanuela.tudorache@umft.ro (E.V.); oancea@umft.ro(C.I.O.)
2 Department of Radiology and Medical Imaging, 'Victor Babes' University of Medicine and Pharmacy Timisoara, Eftimie Murgu Square No. 2, 300041 Timișoara, Romania; dmanolescu@umft.ro(D.L.M.)
3 Department of Computer and Information Technology, Automation and Computers Faculty, "Politehnica" University of Timișoara, Vasile Pârvan Blvd. No. 2, 300223 Timișoara, Romania; laura.broasca@cs.upt.ro(L.B.); versavia.ancusa@cs.upt.ro(V.M.A.); horia.ciocarlie@cs.upt.ro(H.C.)
4 Center for Research and Innovation in Precision Medicine of Respiratory Diseases (CRIPMRD), 'Victor Babes', University of Medicine and Pharmacy, 300041 Timișoara, Romania

* Correspondence: dmanolescu@umft.ro

Diffuse interstitial lung diseases (DILD) are a heterogeneous group of over 200 entities, some with dramatical evolution and poor prognostic. Because of their overlapping clinical, physiopathological and imagistic nature, successful management requires early detection and proper progression evaluation. This paper tests a complex networks (CN) algorithm for imagistic aided diagnosis fitness for the possibility of achieving relevant and novel DILD management data. 65 DILD and 31 normal high resolution computer tomography (HRCT) scans were selected and analyzed with the CN model. The algorithm is showcased in two case reports and then statistical analysis on the entire lot shows that a CN algorithm quantifies progression evaluation with a very fine accuracy, surpassing functional parameters' variations. The CN algorithm can also be successfully used for early detection, mainly on the ground glass opacity Hounsfield Units band of the scan.

Keywords: Interstitial lung disease; Diffuse interstitial lung disease; Idiopathic pulmonary fibrosis; High-resolution computed tomography; Complex Networks; Computer aided diagnosis

1. Introduction

Diffuse interstitial lung diseases (DILD) are a large, heterogeneous group encompassing more than 200 distinct pulmonary disorders, that affect the lung parenchyma within varying degrees, via inflammation and fibrosis [1],[2]. DILD are problematic in the sense that they often present overlapping clinical, radiological and pathological signs and symptoms, yet different evolution patterns, making it difficult to determine the correct diagnostic and treatment, even with a multi-disciplinary approach [3]. Idiopathic pulmonary fibrosis (IPF) is the most frequently encountered DILD [4], a progressive fibrosing interstitial lung disease (PF-ILD), with a distinctively poor outcome and an increased early death risk without treatment [5].

High resolution computer tomography (HRCT) together with biopsy should form the diagnosis foundation, nonetheless the biopsy is often absent, creating the need for accurate diagnosis based solely on visualization [6], [7]. Recent progress on computer aided diagnosis (CAD) techniques [8]–[10] have demonstrated that a mixture of computer enhancements and medical expertise form a synergistic and precise approach. Despite this, some patients are difficult to classify, due to mixed patterns of lung injury and/or interobserver variability, relevant even between experienced radiologists [11].

 doi:10.20944/preprints202208.0099.v1

1.1. DILD early diagnosis

Early detection for certain diffuse interstitial lung diseases is difficult, all the more so when based only on one HRCT. The accuracy in predicting the correct primary diagnosis is improved by the availability of several imaging studies, spaced over time to allow specific findings and patterns representative for the DILD to emerge [12]. This is even more complicated as most DILDs have a variable evolution over time depending on the predominant slope, inflammation (with high potential of reversibility) or fibrosis, while some, like IPF, have an unquestionable progressive nature.

To assist diagnosis, in addition to the HRCT imaging factor, functional lung investigation is indispensable for DILDs diagnosis, monitoring and prognosis. Pulmonary function tests usually show a restrictive disfunction in spirometry, with low forced vital capacity (FVC) in DILD. Novel studies [13] suggest that diffusion capacity of the lungs for carbon monoxide (DLco) correlates to HRCT findings in patients with diffuse parenchymal lung diseases. It should be noted that the decrease in DLco occurs earlier than decrease in FVC so it is a good marker for early lung impairment detection[14].

While composite index predictions for DILD have also been proposed [15], [16] like the modified ILD-GAP score (Gender, Age, Physiology, ILD subtype), integrating clinical-functional elements (respiratory functional tests – Dlco, FVC), they tend to create a mortality prediction model [17] and are used after diagnosis is confirmed, not as an early diagnosis indicator.

1.2. DILDs evolution and imagistic diagnosis

Imagistic diagnosis of DILD is pattern-based and linked to underlying histology. [18] If IPF evolution is indubitable fibrosis, for other DILDs there is considerably more variability in the disease course.

Travis et al [1] proposed five categories for longitudinal behavior patterns divided for ILD evolution. These types of phenotypic clusters in fibrotic DILD can be subdivided into three patterns: stable non-progressive fibrosis after removal of a trigger (e.g.: DILD – drug related), irreversible stable under treatment fibrosis (e.g.: mycophenolate mofetil therapy in connective tissue disease-associated ILD [19] and chronic hypersensitivity pneumonitis [20]) and progressive irreversible fibrosis (IPF-like disease) [21]. Other non-fibrotic DILD cluster can be: reversible self-limiting (respiratory bronchiolitis-associated interstitial lung disease (RB-ILD)) and reversible but with potential for progression (e.g.: cellular non-specific interstitial pneumonia (NSIP) and some fibrotic NSIP, desquamative interstitial- pneumonia (DIP), organizing pneumonia (OP)). This latest longitudinal behavior pattern requires short-term observation to confirm treatment response and long-term observation to ensure that gains are preserved[1].

Fibrotic phenotypes require a constant, long-term follow-up of the HRCT imaging evolution to successfully manage the specific case by maintaining the status, preventing or slowing down the progression[22]. Fibrosis presence is a defining characteristic for a group of progressive lung diseases that includes, but is not limited to IPF, the progressive fibrotic phenotype (PF-ILD)[23]. In radiology terms, usual interstitial pneumonia (UIP) is the classic progressive fibrotic phenotype, but self-sustaining progressive fibrosis is not narrowed only to patients with IPF; because progressive NSIP or chronic hypersensitivity pneumonitis(HPc) phenotype should also be taken into account[24].

Distinguishing the various forms of pulmonary fibrosis is critical for determining correct management and prognosis (e.g.: a patient with a probable UIP pattern has fewer acute exacerbations and longer survival compared to patients with a typical UIP pattern).

1.3. Computer aided diagnosis

There are quite a few approaches to computer aided diagnosis (CAD) for lung HRCTs available or in development, based on different techniques. Whether they are built on artificial intelligence, neural networks or machine learning [8]–[10], these types of soft-

 doi:10.20944/preprints202208.0099.v1

ware applications, fail to capture the dynamics of a pathology evolution. They only provide a static evaluation of HRCTs with no prognosis of a patient's health state. In addition, some of them, like CALIPER, require extra information, such as tests or respiratory parameters, to be able to provide a fairly accurate conclusion (e.g.: affected lung volume), albeit extrapolated in a relatively short timeframe.

A few of these techniques take a more in-depth approach such as analyzing lung patches of certain dimensions [25], however none truly revolutionize the approach to DILD early diagnosis and classification by accurately calculating the deterioration rate and/or affected lung volume.

A mixture of pattern matching and analyzing techniques, the complex network approach[26] might provide insights previously unexplored by the other CADs.

1.4. Hypothesis to be explored

The current paper explores the practical use of a complex networks (CN) analytical approach based on [26] and its suitability to provide early discovery and/or support/enhance clinical diagnosis by offering a reliable quantifiable progression metric.

Hypothesis 1 states that the CN algorithm accurately characterizes quantitatively DILD progression.

Hypothesis 2 advances that the CN algorithm allows early detection

2. Materials and Methods

2.1. Lot selection

From the private 'Dr. Victor Babes' Infectious Diseases and Pneumoftiziology Clinical Hospital Timisoara National Fibrosis Center database were selected 65 DILD and 31 normal lung patients with multiple scans.

The lots were similar in age and sex profile, and they all legally consented to their data being used for academic purposes and the Ethics Committee approved this study.

For each patient physiological data (age, sex, smoking status), pulmonary function tests (PFT) – like forced vital capacity (FVC) by spirometry performed and diffusing capacity of the lungs for carbon monoxide (DLco) together with HRCT annotations were investigated. Patients' quantitative dynamic HRCT images were also provided and their case history was reviewed by four pneumology specialists.

Since each scan in the database is already annotated by at least three specialists, it was possible to define very selective criteria for the DILD lot: typical HRCT appearance of the most commonly encountered interstitial lung diseases in which overlapping of primary lesions creates models for idiopathic pulmonary fibrosis (IPF), non-specific interstitial pneumonia (NSIP), hypersensitivity pneumonitis (HP), sarcoidosis(S) and organizing pneumonitis (OP). To narrow the scope, the selected primary lesions were reticulation and consolidation (defined together as band C), ground glass opacity (band GGO) as well as emphysema and cysts (defined together as band E). These lesions have clear imagistic absorption rates, that permit grouping, further explained in section 2.3.

The HRCT region of interest was marked by a radiologist with high experience in imagistic diagnosing of DILDs (10+ years), collaborated with the other specialists' inputs. The selected imagistic elements were typical for IPF, NISIP, HP, S and OP. Since the morphological pattern of IPFs represents 55% of idiopathic interstitial pneumonia, the selected cases presented usual interstitial pneumonia pattern – subpleural and peripheric distribution, with apico-basal gradient (predominantly basal) of reticulations, bronchiolectasis and end stages "honeycombing" cysts with paucity of ground glass opacification [27], [28]. An IPF subtype characterized by low survival rate, the combined pulmonary fibrosis and emphysema (CPFE) was also pursued [29].

In NSIP cases, features of cellular type with lower lung predominant subpleural ground glass opacification and fine reticulations were provided [30]. Also, cases in the

 doi:10.20944/preprints202208.0099.v1

fibrotic stage, with reticulation, traction bronchiectasis, and architectural distortion due to fibrosis were selected.

Lesion to be found for the acute HP cases were centrilobular or geographical ground glass opacification, poorly defined centrilobular nodules and air trapping (mosaic attenuation) with characteristic mid- and upper-lung zone predominance[31]. Additionally, chronic HP cases with fibrosis with septal thickening – reticulation, traction bronchiectasis, possibly honeycombing and headcheese sign (various degrees of ground-glass and marked mosaic attenuation due to sparing of secondary lobules) [32] were also carefully chosen.

In sarcoidosis, the lot presented, perilymphatic micronodularity. Moreover, the lot was selected to be in sarcoidosis fibrotic stage with reticulation and/or honeycombing [33] presence.

The OP cases had bilateral patchy airspace consolidation/ground-glass opacities, with or without small nodules, with typical perilobular pattern and fluctuation[34],[35].

2.2. Imaging parameters

The patients were analyzed with constant settings, on the General Electrics (GE) Healthcare Optima 520 CT, using sixteen 1.25 mm thick slices, reconstructed using high spatial frequency at 32. The scan time was 1 second and was performed with the following settings: 120 kV, 130 mAs, with a 2.5 mm collimation. The field of view was 35 cm with a 768x768 matrix size. The radiation dose was adapted as needed, due to tissue penetration.

The examination position was prone for the 90% of the selected lot, the rest being analyzed in a supine position.

Examinations were stored using the industry accepted format of Digital Imaging and Communications in Medicine (DICOM) in the cloud storage of the aforementioned National Fibrosis Center database

2.3. Selecting the pathological imagistic alterations

Literature defines four categories of pathological imagistic lung alterations: the reticular pattern, nodular pattern, high attenuation (ground glass opacity, consolidation, atelectasis) and low attenuation (emphysema, cyst, air trapping) whose distribution, overlap, and association with other lesions matter, in relation to the secondary pulmonary lobule (SPL) and the lung regions segmentation [36], [37]. However, attenuation range of X-ray beam tissue absorption, measured in Hounsfield Units (HU) and reflected in the grey tones from the image can help with the layering of these lesions. For the used CT apparatus, General Electric Healthcare Optima 520 literature [38],[39],[40] shows that three HU bands can encompass all of the aforementioned lung alterations: band E [-1024, -977), band GGO [-977, -703) and band C [-100, 5).

On band E, emphysema appears as polygonal or rounded low-attenuation areas , without walls [41] and on the same band, cysts are round circumscribed area of lucency or low attenuation with a diameter greater or equal to 1 cm, surrounded by epithelial or fibrous contour, typically presenting discrete walls [42].

Ground-glass opacity (GGO) refers to a homogeneous area of increased lung opacity (a process which partially fills the airspaces) in which the increased opacity does not obscure the underlying bronchial and vascular structures. GGO may either be the result of air space disease (partial filling of the alveoli) or early interstitial lung disease (fine thickening of the interstitium or alveolar wall - i.e. fibrosis) because of fluid, cells and fibrosis presence [43]. This pattern has its own HU band and is therefore easier to select.

Consolidation is denser than GGO and from a purely visual viewpoint, consolidation looks like a visibly defined compact opacity in DILD [44]. On the same HU band as consolidations is the reticular pattern, a network of intersecting lines opacities. The reticulation appears due to interstitium injury causing thickening of the intra and interlobular septa of secondary pulmonary lobule [28] pathologically reflected in the various degrees of inflammation and fibrosis.

 doi:10.20944/preprints202208.0099.v1

In imaging practice, the basic lesions in the DILD appearance may exist independently, but most often they are found in various combinations, overlapping , creating true models that may be typical or less for a certain DILD entity [45], [46] . Mosaicism [47], head cheese pattern [48], crazy paving pattern [49] are examples of this overlap, but more important for this research paper is the honeycombing pattern which is a mixture of a cluster cysts (E band) and reticulations (C band) [50]. Pathologically, honeycombing is the final stage in DILD progression to fibrosis with architectural distortion, traction bronchiolectasis and cysts layers formation [43] [51]. An algorithm splitting these lesions on separate layers can therefore enhance the data.

2.4. Computer-enhancing the data

The transformation of DICOM images by the studied algorithm [26] takes place in multiple stages: First DICOM images are analyzed and each pixel is converted into its HU unit equivalent. Then, depending on the desired HU bands, only pixels pertaining to said bands are kept, eliminating all other. The remaining pixels are split into layers according to their specific HU band, obtaining one separate image for every layer respectively. The resulting images are then transformed into complex networks according to specific predefined attachment rules, in a manner similar to conversion of grayscale images into complex networks presented in [52], [53], [54]: nodes with similar HU values (within the range of 50 HU units) and closer than 4px away are considered to be linked, while all noncompliant ones are detached. In other words, any two visual points in the lung which are very close together and have a similar shade (density), are very probably part of the same type of tissue, whether it is affected or healthy. Based on the obtained network, certain metrics can be calculated and consequently, more precise conclusions can be drawn regarding the structure of the analyzed lung area.

From the DICOM format, for each selected region of interest, three complex networks were generated, one for each pathologically relevant Hounds-field Units (HU) interval: E for emphysema and cysts, GGO for ground glass opacity and C for consolidation and reticulations. The scale for the HU transformation is device-specific and was based in this implementation on [38],[39],[40].

2.5. Selecting relevant metrics

In order to assess the usefulness of the proposed CN approach, the measurements should reflect the underlying biological processes and their dynamic evolution. A CN can be characterized by many metrics, from the ones that measure the way it is interconnected, to the ones that characterize information flow or clusterization [55]. Since the underlying purpose of this paper can be biologically translated into a way to measure lesions and their expansion, the corresponding CN measurements should then reflect interconnectedness and size. Therefore, the selected measurements are: maximum degree number (the maximum connections number in the network for a singular node), total degree count (how many connections are in the network) and average degree count (the average number of connections per node – how sparse the network is). A network node can represent either a singular pixel or a small region, according to the way the algorithm is implemented and for the purpose of this section it echoes a pixel.

Preprints (www.preprints.org) | NOT PEER-REVIEWED | Posted: 4 August 2022 doi:10.20944/preprints202208.0099.v1

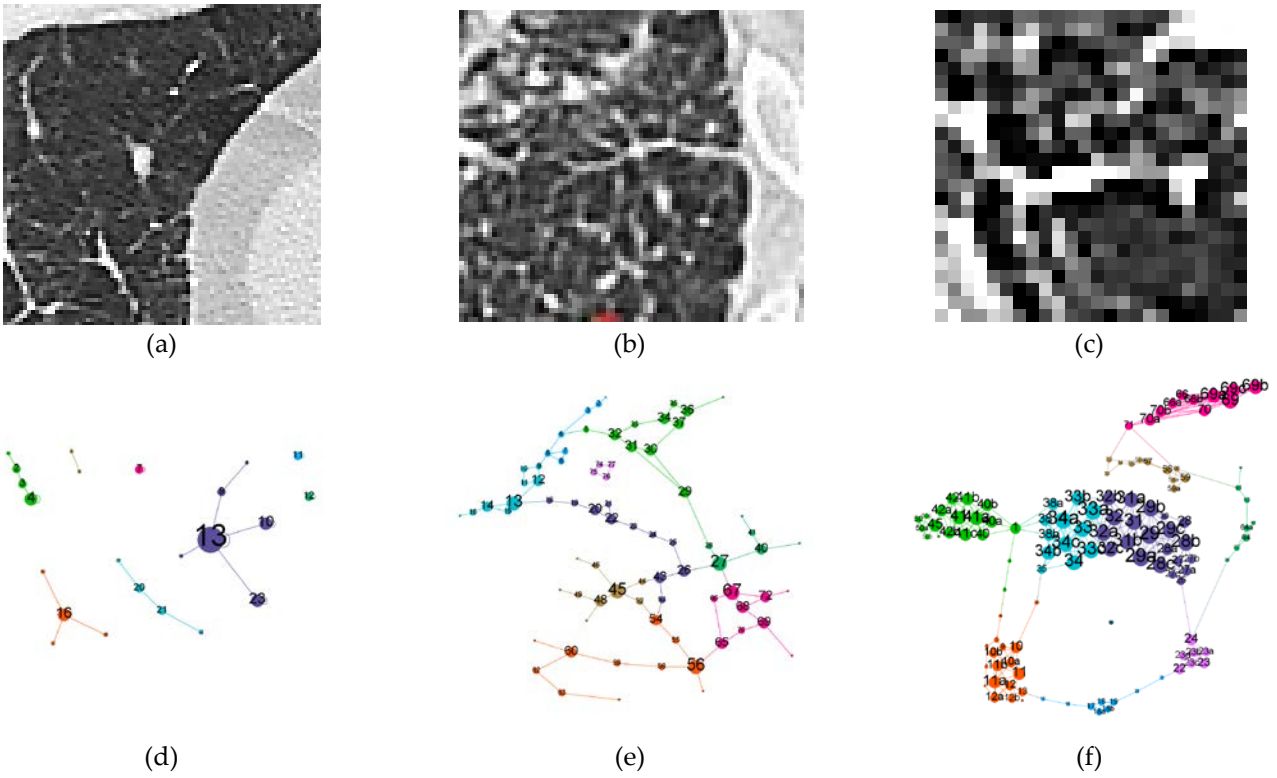

Figure 1 Simple example to illustrate CN measurements and biological counterparts
(a) CT section with a micronodule in center (b) CT section with sarcoidosis(perilymphatic micronodules) (c) CT section with honeycombing cysts (d) CN depicting micronodule CT (e) CN depicting sarcoidosis CT (f) CN depicting honeycombing CT
For all CNs, node positions mimic light color entities on the CT above them, node size is proportional to node degree and on each node a numeric label is provided. Label size is proportional to node size. Maximum, minimum and scaling for node size is constatnt in all three CNs. Node color reflects clusterisation, provided for visual interest only. Edge width depiction is constant. CT slice scale between a, b and c is not the same as this is intended for CN exemplification only.

Figure 1 shows examples to illustrate these specific measurements. A micronodule (Figure 1a) can be translated visually (Figure 1d) as a node or a cluster of nodes (e.g.: Figure 1d – node number 13 - purple) with the highest degree in the analyzed window. A sarcoidosis or a honeycombing network (Figure 1b and c) may have similar total number of edges (interconnections), yet their average degree metrics are wildly different. One (S – Figure 1b) has many nodes with a median of approximately two connections (reflecting the typical micronodules perylimphathic distribution of linearly interconnected nodules, like a string), yet the other one (honey combing – Figure 1c) has fewer nodes but with many connections, averaging at 5.8 (reflecting the cyst wall, which is linearly homogenous). Loosely translated, total count shows how "damaged" the sample is per total, average count shows how localized these lesions are and maximum degree represents the pathological alteration's peak intensity. Therefore, it can be concluded that these measurements reflect interconnectedness and size, the two parameters needed to be measured, obviously evaluated separately on all three HU bands.

For progression assessment, the same patients were analyzed in successive scans. Adjusting for as close as possible anatomical continuity, the selected (quasi) identical locations were compared on the three HU bands. Since progression is translated as a variation over time, this interprets into the engineering notion of speed. However, measurement difference over time reflects an absolute speed, characteristic for a specific location / patient and since the measurement should be comparable between individuals/ scans, a relative variation speed was defined, as expressed in equation (1).

Preprints (www.preprints.org) | NOT PEER-REVIEWED | Posted: 4 August 2022 doi:10.20944/preprints202208.0099.v1

$$v = \begin{cases} \frac{(s-s_0)}{s_0 * t}, for\ s_0\ != 0 \\ \frac{s}{t},\ in\ rest \end{cases}. \quad (1)$$

The s value from (1) represents the analyzed metric and s_0 is the corresponding point from the reference sample, used for normalization.

In Equation (1) t is expressed as years, since DILD patients require yearly checks [56]. A simple way to compute its value is by counting the number of days (for example by using the Excel function DAY ()) between the oldest HRCT (at time t_0) and the one currently evaluated (t_1) and normalizing it using a 365 days year.

$$t = DAY\ (DATE\ (t_1) - DATE(t_0))/365. \quad (2)$$

Another valid option is to normalize the year at 360 days as it is customary in some financial formulas, yet the most aspect is the constancy of the normalization type. In this paper, the normalization provided in formula (2) was used.

3. Results

3.1. Case reports

To better illustrate the process this section presents sample locations from two very different patients put through the analysis process. The results in Figure 2 illustrate typical UIP+ emphysema (CPFE phenotype) imagistic progression.

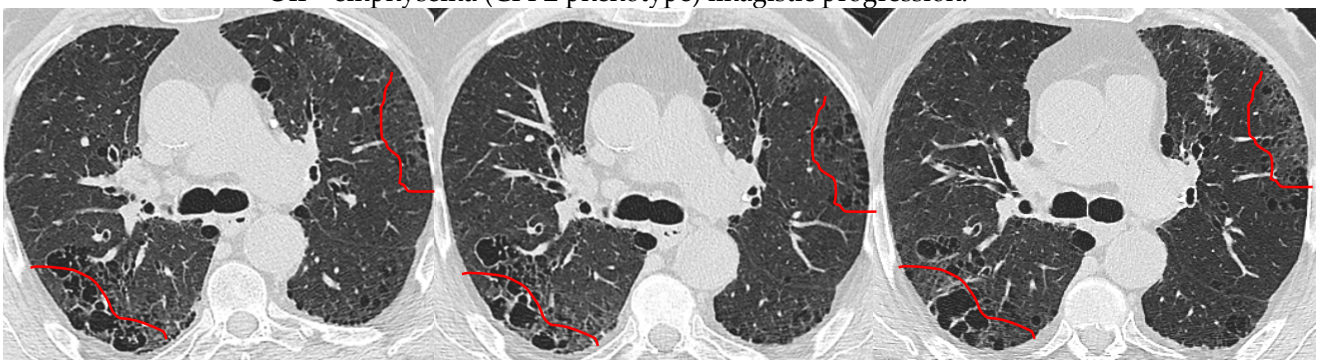

(a) (b) (c)

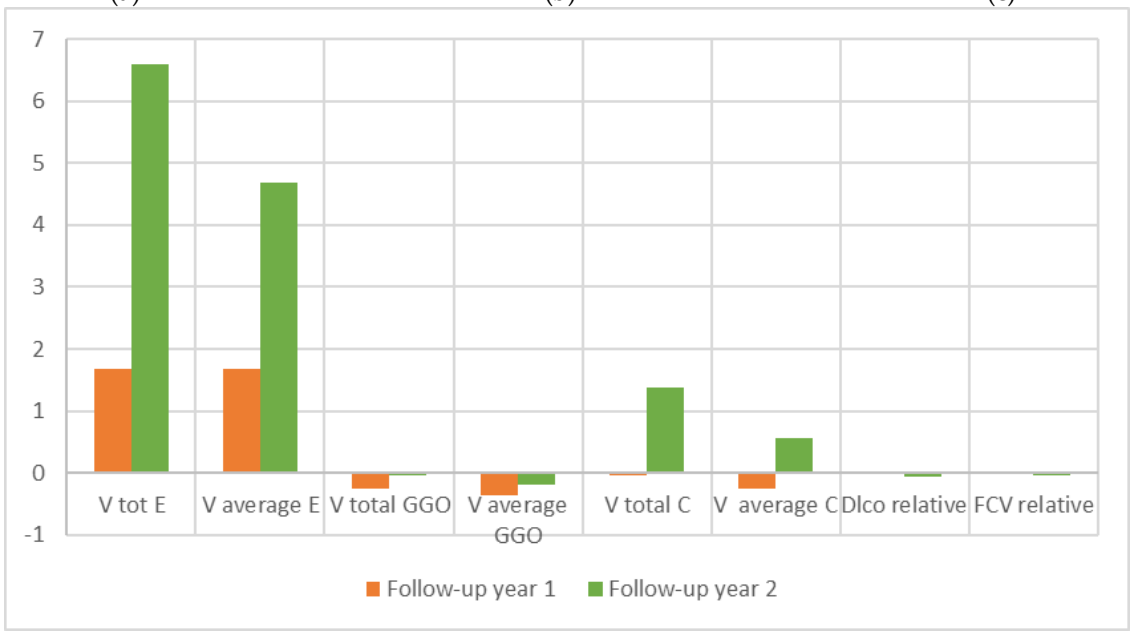

(d)

Preprints (www.preprints.org) | NOT PEER-REVIEWED | Posted: 4 August 2022 doi:10.20944/preprints202208.0099.v1

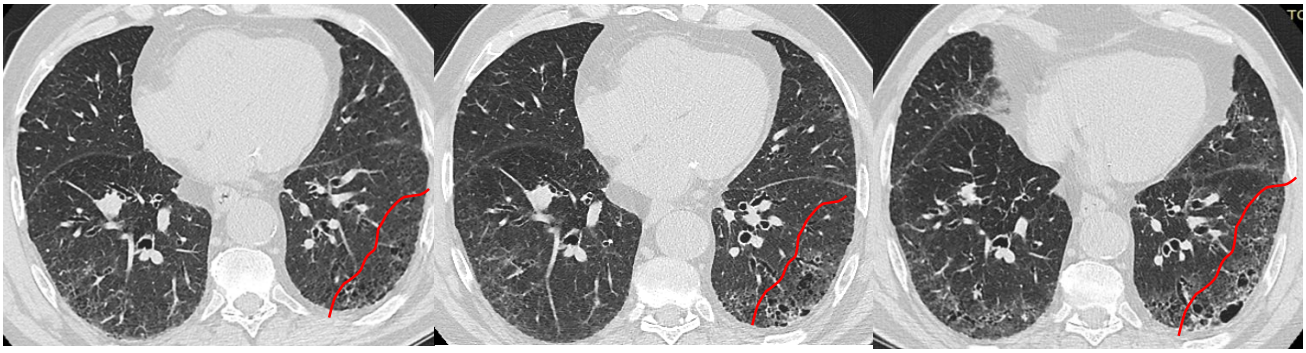

(e) (f) (g)

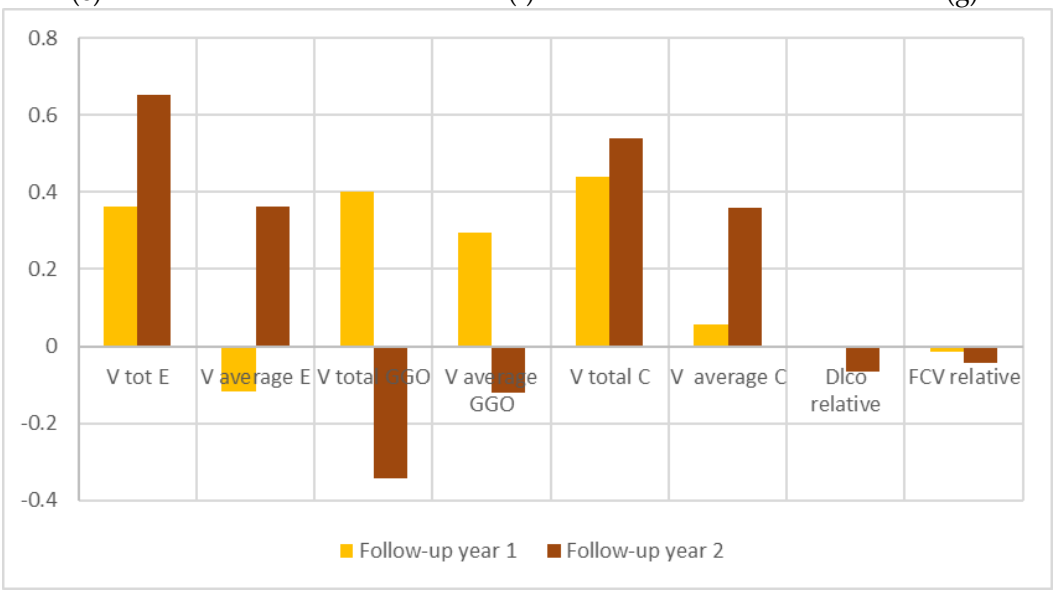

(h)

Figure 2. Case report for an lung axial HRCT,UIP+E pattern(CPFE) patient progression .
(a) Superior lung region HRCT slice in initial t_0 year (b) Superior lung region HRCT slice in next year – t_1 (c) Superior lung region HRCT slice in second year – t_2 (d) Relative speed variations on the superior lung slice, for all three bands
(e) Basal lung region HRCT slice in initial t_0 year (f) Basal lung region HRCT slice next year – t_1 (g) Basal lung region HRCT slice in second year – t_2 (h) Relative speed variations on the basal lung slice, for all three bands

The results presented in Figure 3 present a typical NSIP pattern in evolution.

(a)

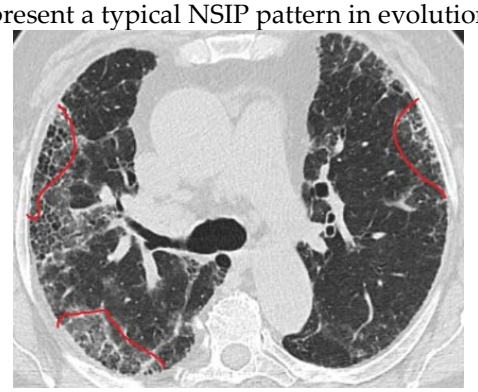

(b)

Preprints (www.preprints.org) | NOT PEER-REVIEWED | Posted: 4 August 2022 doi:10.20944/preprints202208.0099.v1

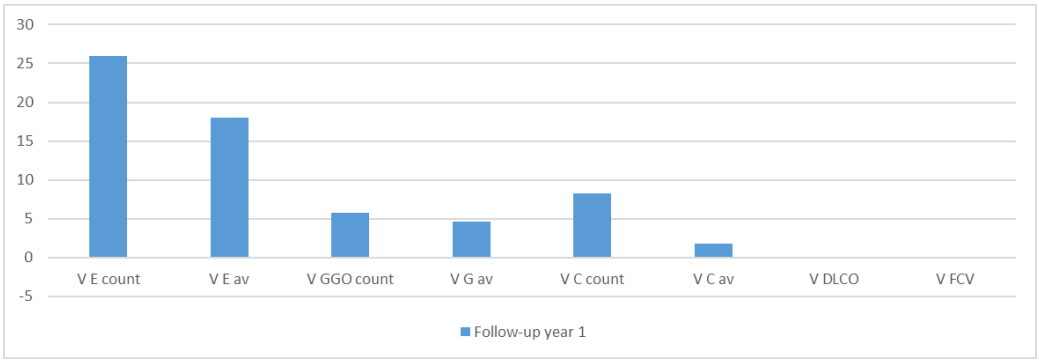

(c)

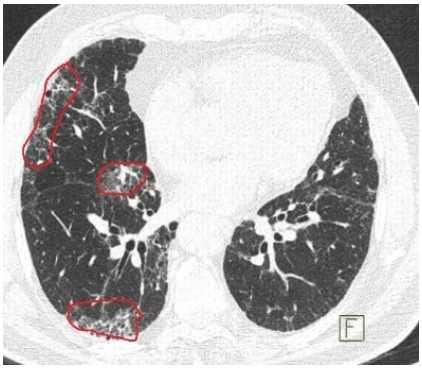

(d)

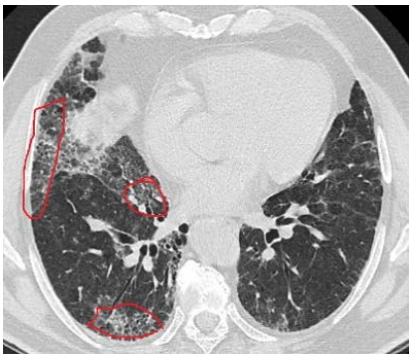

(e)

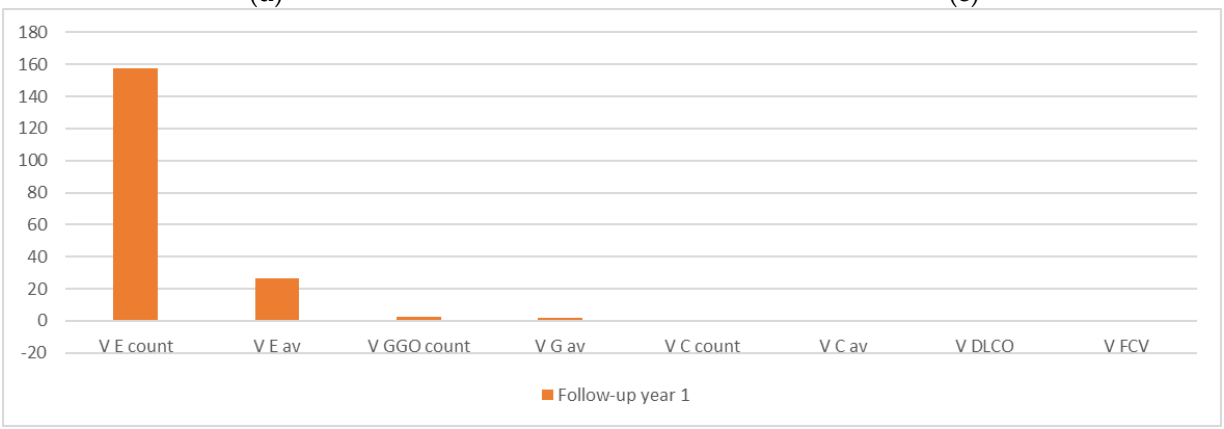

(f)

Figure. 3. Case report for a NSIP+E patient progression
(a) Superior lung region axial HRCT slice in initial t_0 year (b) Superior lung region axial HRCT slice in next year – t_1
(c) Relative speed variations on the superior lung slice, for all three bands
(d) Basal lung region axial HRCT slice in initial t_0 year (e) Basal lung region axial HRCT slice in next year – t_1
(f) Relative speed variations on the basal lung slice, for all three bands

3.2. Progression speed

In a manner similar to the one presented in the previous section the whole lot was analyzed. The defined relative speed, on each HU band and on each CN, parameter analyzed with a t-test versus DLco relative variation is shown in Table 3.5. The lot on which this test was performed is the entire lot, normal and DILDs patients. It should be noted that, while maximum degree can also be analyzed, since the measurement searched for is progression, peak singular lesion is less relevant.

Table 1. T test results for relative speed in HU bands parameters VS DLco

Preprints (www.preprints.org) | NOT PEER-REVIEWED | Posted: 4 August 2022 doi:10.20944/preprints202208.0099.v1

HU Layer	Total count VS DLCO	Average count VS DLco	Parameters
E	1.81144865	*2.297734923*	t Stat
	0.038529988	*0.013194925*	P(T<=t) one-tail
	2.016692199	*2.015367574*	t Critical two-tail
GGO	-1.334981884	-1.82528253	t Stat
	0.092702764	0.035714932	P(T<=t) one-tail
	1.987934206	1.987934206	t Critical two-tail
C	-1.334981884	-1.82528253	t Stat
	0.093421672	0.035996812	P(T<=t) one-tail
	1.999623585	1.992543495	t Critical two-tail

The null hypothesis is retained for all but one of the selected series. The average count VS Dlco test on the E band rejects the null hypothesis and its data are marked with italics in Table 1.

3.3. Testing for early detection

To search for early detection, the lot was grouped into cases considered normal and cases with incipient DILD and fairly good functional parameters (GAP-ILD 0–3 points, DLco values between 70 and 85%). The DLco values were chosen as an interval centered on the lower normal limit (80%) to allow the inclusion of early impairment in alveolar-capillary membrane. The cases were analyzed on the same three axis with results presented as box plots in Figure 4 and resumed in Table 2.

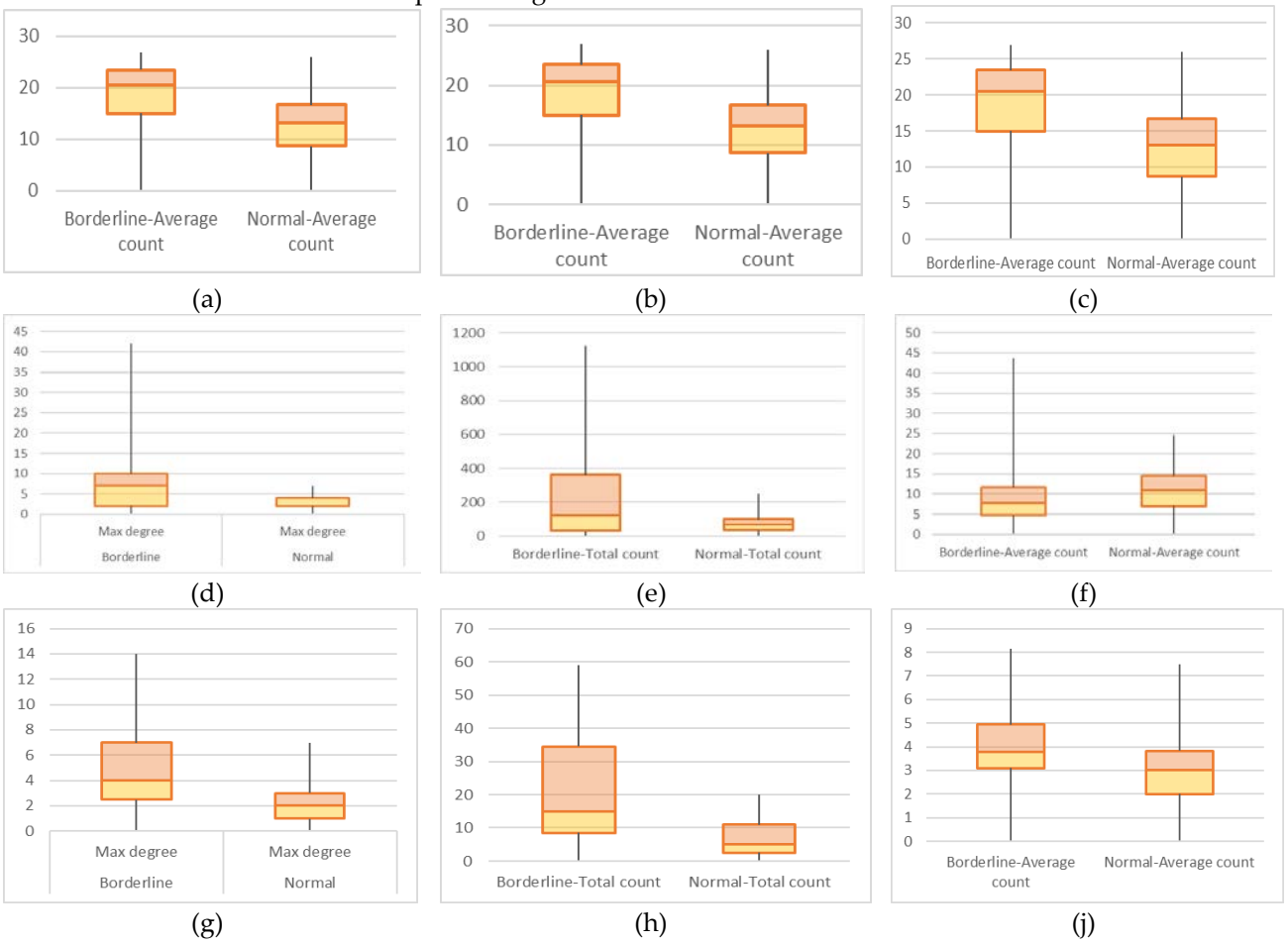

Figure 4 CNs on Borderline normal versus normal layer distribution;
Layer E values with (a) Maximum degree (b) Total count (c) Average count;

 doi:10.20944/preprints202208.0099.v1

Layer GGO values with (d) Maximum degree (e) Total count (f) Average count;
Layer C with (g) Maximum degree (h) Total count (i) Average count

The t-test data presented in table 2 is written in italics for the series rejecting the null hypothesis.

Table 2. Statistical t-tests results between borderline and normal lungs

Layer	Max Degree	Total count	Average count	Parameters
E	-0.357327012	-0.33960631	-1.194455411	t Stat
	0.361362738	0.367964892	0.119667428	P(T<=t) one-tail
	2.02107539	2.02107539	2.02107539	t Critical two-tail
GGO	*2.362901118*	*2.496174465*	*2.132901092*	t Stat
	0.016568972	*0.012345754*	*0.023097162*	P(T<=t) one-tail
	2.144786688	*2.131449546*	*2.093024054*	t Critical two-tail
C	*2.787128882*	*2.910253494*	1.723111496	t Stat
	0.006593367	*0.005384188*	0.048371727	P(T<=t) one-tail
	2.119905299	*2.131449546*	2.055529439	t Critical two-tail

4. Discussion

Figure 2 presents two levels of axial HRCT slices (superior and basal lung region) selected in order to showcase typical UIP+ emphysema (CPFE phenotype) imagistic progression. It should be mentioned that although all the results presented in this paper pertain to the axial lung plane, this does not restrict their generality. A technical analysis presenting the equivalence in sagittal, coronal and axial planes results, would overstate the purpose of this paper, which is to showcase CN model applications in imagistic settings. Returning to the UIP + emphysema case, an imagistic interpretation for the progression starts with the initial t_0 point which, in superior lung region indicates fine reticulation presence, bullous emphysema and slight subpleural honeycombing cysts and in basal region is marked with reticulation and honeycombing lesions, both sparce.

As was previously mentioned, according to the HU ranges, reticulations and consolidations have similar values, yet in this specific context the values are interpreted as reticulations. In the selected areas, the CN model offers data for relative variation speed on each layer. This speed is specific to a selected site and reflects a relative variation in characteristics over a time period. It is not an absolute value, its meaning is related to the swiftness of change, therefore highlighting rapidly deteriorating areas. Since the algorithm behind the CN conversion considers lesions as small as 3 mm [26], by default, the speed is more granular than human eye.

The CN model's relative speed on the E layer presents an increase in follow up year 1 and year 2, yet the magnitude between the superior (Figure 2.d) and basal slices (Figure 2. h) is very different. The superior region is almost 10 time faster deteriorating than the basal slice, quantifying superior lobe's emphysema lesion extension and honeycombing cyst layers increase (Figure 2 a, b and c) compared with the basal lobe in which emphysema is not very well expressed (Figure 2 e, f and g). C layer increases both on the superior slice and basal slice, presenting the pathological process of lesion progression with lung architectural distortion, reticulation, multilayer variate size cyst. The model detects small variations on the GGO, especially in the basal plane (Figure 2 e,f,g, h), suggesting a probable acute substrate in that specific area. This image is highly annotated (being part of the national DILD database, is already rated by at least 3 lung experts and 5 other lung specialists rated all the images used in this study), yet the GGO difference is imperceptible. Studying the patients' data, the symptoms from follow-up year 1 are inexplicably slightly exacerbated, yet they are not so in follow-up year 2. This confirms the CN relative speed light variation and its ability for early detection. Functional parameter relative variation

Preprints (www.preprints.org) | NOT PEER-REVIEWED | Posted: 4 August 2022 doi:10.20944/preprints202208.0099.v1

is almost zero in both follow-up years, defining a stationary functional status, underling the premature detection of the proposed CN model.

Figure 3 presents imagistic axial lung HRCT lesion evolution in a NSIP pattern case. On the E band, relative speed expresses a marked increase in the emphysema focus points numbers (total count), with only medium increase in their intensity (average), for both sample sites, clearly explained by the buildup in honeycombing cysts layers. GGO in t_0 (Figure 3 a and d) shows slightly increase in the follow-up sample, corresponding with the imaging slice HRCT interpretation (Figure 3 c, f). The C layer displays only on superior regions a slight increase (Figure 3 a, b), reflected by the well-defined multilayer cysts and their defining walls. Again, functional parameters have almost no variation, underling the premature detection of the proposed CN model.

Referring to the entire lot, results from Table 1 support the testing of hypothesis 1 which states that the CN algorithm accurately and quantitatively characterizes DILD progression. The fact that most of the statistical comparison between Dlco and CN measurements variation show relevant similarities, concludes that hypothesis 1 is true. The only exception belongs to the comparison between average count and DLco on the E band (marked with italic in the table). Some patients classified as normal have chronic obstructive lung pathology in a compensation clinical status and /or are active or former smoker. Since the CN measurements reflect biological terms, this means that the number of the E-layer regions of interest are the same but the regions' median intensity is statistical relevant higher than its corresponding functional parameter variance.

The statistical testing between the borderline and normal groups, presented in Figure 4 and Table 2 warrants further exploration. On the E layer there is no statistical difference between the early diagnostic set and the normal set, therefore the CN model does not allow early detection on this layer. From a biological perspective, early DILD diagnosis with emphysema phenotype is almost identical to smokers' emphysema lesions, as confirmed by the results. On the GGO layer, there is a statistical difference, the null hypothesis is rejected, and the proposed model is successful in early DILD detection. On the C band maximum degree and total count detect early DILD, yet average count does not. Pathologically, the proposed model accurately detects well defined consolidation lesions and does not successfully differentiate diffuse early consolidations with blurred edges in their early stages. As a consequence, hypothesis 2 that the CN algorithm allows early detection is true on the GGO, mostly true on C layer and false on the E layer.

5. Conclusions

To successfully deal with DILDs there are two issues needed to be solved, well known by all the practicians: early detection and accurate progression evaluation. So far, the traditional medical and the computer-based approaches based on artificial intelligence, machine learning, etc., have both come up short even though some diseases like IPF critically need efficient solutions. The purpose of this paper was to explore if a CN based computer aided diagnosis can provide the much-required data needed to successfully manage DILDs.

In order to do so, two hypotheses were tested: first one explored progression and the second one early detection. For progression, the CN CAD was an almost complete success. Its fine accuracy, in testing lesions as small as 3 mm, allowed correlation with the clinical status beyond the granularity of standard functional tests. The only problem was on the E band for the average count measurement type, yet this is easily offset by the other 5 measurement axis.

For early detection, the inflammation GGO layer proved to be key. In fact, inflammation and fibrosis are the two typical DILD states, and the CN algorithm performed well on both GGO and C defined HU bands. This showcases practical abilities of this algorithm

 doi:10.20944/preprints202208.0099.v1

type, particularly well-suited to DILDs, not filled so far by any other tools, like for example Caliper.

As pitfalls, the CN algorithm has a considerable run-time, growing exponentially proportional with the analyzed window. It also needs prior lung segmentation, that can be obtained through other CAD or manually.

It is the authors' belief that this algorithm should be incorporated in a much larger CAD, combining the faster machine learning segmentation and pattern detection capabilities with the slower, yet accurate CN local analysis.

Supplementary Materials: The datasets generated or analyzed within the current research study are available from the corresponding author on reasonable request.

Author Contributions: Conceptualization, A.A.T., V.M.A. and L.B.; methodology, V.M.A.; software, L.B.; validation D.L.M. ; formal analysis, L.B. and V.M.A.; investigation, A.A.T., L.B., and V.M.A; resources D.L.M and C.I.O. ; data curation E.V. and C.C.P.; image sample selection: A.A.T, C.I.O, D.L.M, E.V, C.C.P; writing—original draft preparation, A.A.T, V.M.A., and L.B; writing—review and editing, A.A.T, V.M.A., and L.B.; visualization, L.B. and V.M.A; supervision, H.C., C.I.O, D.L.M; project administration, C.I.O.; All authors have read and agreed to the published version of the manuscript.

Funding: This research received no external funding

Institutional Review Board Statement: The study was conducted in accordance with the Declaration of Helsinki, and approved by the Ethics Committee of Clinical Hospital for Infectious Diseases and Pneumoftiziology Dr. Victor Babeș Timișoara (protocol code 11835/26.11.2021) for studies involving humans.

Informed Consent Statement: Informed consent was obtained from all subjects involved in the study.

Data Availability Statement: The data presented in this study are available on reasonable request from the corresponding author.

Conflicts of Interest: The authors declare no conflict of interest.

References

[1] W. D. Travis *et al.*, "An Official American Thoracic Society/European Respiratory Society Statement: Update of the International Multidisciplinary Classification of the Idiopathic Interstitial Pneumonias," *Am. J. Respir. Crit. Care Med.*, vol. 188, no. 6, pp. 733–748, Sep. 2013, doi: 10.1164/rccm.201308-1483ST.

[2] K. C. Meyer, "Diagnosis and management of interstitial lung disease," *Transl. Respir. Med.*, vol. 2, p. 4, Feb. 2014, doi: 10.1186/2213-0802-2-4.

[3] S. Tomassetti, C. Ravaglia, and V. Poletti, "Diffuse parenchymal lung disease," *Eur. Respir. Rev.*, vol. 26, no. 144, p. 170004, Jun. 2017, doi: 10.1183/16000617.0004-2017.

[4] B. Guo *et al.*, "The interstitial lung disease spectrum under a uniform diagnostic algorithm: a retrospective study of 1,945 individuals," *J. Thorac. Dis.*, vol. 12, no. 7, pp. 3688–3696, Jul. 2020, doi: 10.21037/jtd-19-4021.

[5] "American Thoracic Society. Idiopathic pulmonary fibrosis: diagnosis and treatment. International consensus statement. American Thoracic Society (ATS), and the European Respiratory Society (ERS)," *Am. J. Respir. Crit. Care Med.*, vol. 161, no. 2 Pt 1, Art. no. 2 Pt 1, Feb. 2000, doi: 10.1164/ajrccm.161.2.ats3-00.

[6] K. C. Meyer, "Diagnosis and management of interstitial lung disease," *Transl. Respir. Med.*, vol. 2, p. 4, Feb. 2014, doi: 10.1186/2213-0802-2-4.

[7] D. Manolescu, L. Davidescu, D. Traila, C. Oancea, and V. Tudorache, "The reliability of lung ultrasound in assessment of idiopathic pulmonary fibrosis," *Clin. Interv. Aging*, vol. 13, pp. 437–449, 2018, doi: 10.2147/CIA.S156615.

[8] K. Simonyan and A. Zisserman, "Very Deep Convolutional Networks for Large-Scale Image Recognition," *ArXiv14091556 Cs*, Apr. 2015, Accessed: Feb. 06, 2022. [Online]. Available: http://arxiv.org/abs/1409.1556

[9] Q. Li, W. Cai, X. Wang, Y. Zhou, D. D. Feng, and M. Chen, "Medical image classification with convolutional neural network," in *2014 13th International Conference on Control Automation Robotics Vision (ICARCV)*, Dec. 2014, pp. 844–848. doi: 10.1109/ICARCV.2014.7064414.

[10] S. L. F. Walsh, L. Calandriello, M. Silva, and N. Sverzellati, "Deep learning for classifying fibrotic lung disease on high-resolution computed tomography: a case-cohort study," *Lancet Respir. Med.*, vol. 6, no. 11, Art. no. 11, Nov. 2018, doi: 10.1016/S2213-2600(18)30286-8.

[11] A. A. Trusculescu, D. Manolescu, E. Tudorache, and C. Oancea, "Deep learning in interstitial lung disease—how long until daily practice," *Eur. Radiol.*, vol. 30, no. 11, Art. no. 11, Nov. 2020, doi: 10.1007/s00330-020-06986-4.

[12] H. Hatabu, G. M. Hunninghake, and D. A. Lynch, "Interstitial Lung Abnormality: Recognition and Perspectives," *Radiology*, vol. 291, no. 1, pp. 1–3, Apr. 2019, doi: 10.1148/radiol.2018181684.

[13] E. G. Hieba, E. E. Shaimaa, S. S. Dina, and A. O. Noha, "Diffusion lung capacity for carbon monoxide correlates with HRCT findings in patients with diffuse parenchymal lung disease," *Egypt. J. Bronchol.*, vol. 14, no. 1, p. 39, Nov. 2020, doi: 10.1186/s43168-020-00042-x.

[14] V. Cristian Oancea Ovidiu Fira-Mlădinescu Voicu Tudorache, "Tratat de Pneumologie pentru medici rezidenti.," in *Capitolul 3 .Metode de investigatie imagistica a patologiei pulmonare*, pp. 42–59.

[15] S. H. Lee *et al.*, "Comparison of CPI and GAP models in patients with idiopathic pulmonary fibrosis: a nationwide cohort study," *Sci. Rep.*, vol. 8, no. 1, p. 4784, Mar. 2018, doi: 10.1038/s41598-018-23073-3.

[16] C. Hyldgaard, O. Hilberg, and E. Bendstrup, "Validation of GAP score in Danish patients diagnosed with idiopathic pulmonary fibrosis," *Eur. Respir. J.*, vol. 42, no. Suppl 57, Sep. 2013, Accessed: Jun. 15, 2022. [Online]. Available: https://erj.ersjournals.com/content/42/Suppl_57/P2367

[17] C. J. Ryerson *et al.*, "Predicting Survival Across Chronic Interstitial Lung Disease: The ILD-GAP Model," *CHEST*, vol. 145, no. 4, pp. 723–728, Apr. 2014, doi: 10.1378/chest.13-1474.

[18] S. L. F. Walsh and M. Kolb, "Radiological diagnosis of interstitial lung disease: is it all about pattern recognition?," *Eur. Respir. J.*, vol. 52, no. 2, Aug. 2018, doi: 10.1183/13993003.01321-2018.

[19] "Mycophenolate mofetil improves lung function in connective tissue disease-associated interstitial lung disease - PubMed." https://pubmed.ncbi.nlm.nih.gov/23457378/ (accessed Jun. 20, 2022).

[20] J. Morisset *et al.*, "Use of Mycophenolate Mofetil or Azathioprine for the Management of Chronic Hypersensitivity Pneumonitis," *Chest*, vol. 151, no. 3, pp. 619–625, Mar. 2017, doi: 10.1016/j.chest.2016.10.029.

[21] G. Raghu *et al.*, "An official ATS/ERS/JRS/ALAT statement: idiopathic pulmonary fibrosis: evidence-based guidelines for diagnosis and management," *Am. J. Respir. Crit. Care Med.*, vol. 183, no. 6, pp. 788–824, Mar. 2011, doi: 10.1164/rccm.2009-040GL.

[22] SOCIETATEA ROMÂNÃ DE PNEUMOLOGIE, GRUPUL DE LUCRU PENTRU PNEUMOPATII INTERSTIÞIALE DIFUZE, and ªI SARCOIDOZÃ, "Ghid de diagnostic si tratament al PID," 2015. https://www.srp.ro/ghiduri/Ghid%20de%20diagnostic%20si%20tratament%20al%20PID.pdf (accessed Feb. 06, 2022).

[23] A. U. Wells, K. K. Brown, and V. Cottin, "The progressive fibrotic phenotype in current clinical practice," *Curr. Opin. Pulm. Med.*, vol. 27, no. 5, pp. 368–373, Sep. 2021, doi: 10.1097/MCP.0000000000000805.

[24] W. A. Wuyts, A. Cavazza, G. Rossi, F. Bonella, N. Sverzellati, and P. Spagnolo, "Differential diagnosis of usual interstitial pneumonia: when is it truly idiopathic?," *Eur. Respir. Rev.*, vol. 23, no. 133, pp. 308–319, Sep. 2014, doi: 10.1183/09059180.00004914.

[25] Q. Li, W. Cai, and D. D. Feng, "Lung image patch classification with automatic feature learning," *Annu. Int. Conf. IEEE Eng. Med. Biol. Soc. IEEE Eng. Med. Biol. Soc. Annu. Int. Conf.*, vol. 2013, pp. 6079–6082, 2013, doi: 10.1109/EMBC.2013.6610939.

[26] L. Broască *et al.*, "A Novel Method for Lung Image Processing Using Complex Networks," Jul. 2022, doi: 10.20944/preprints202207.0156.v1.

[27] S. Hobbs, J. H. Chung, J. Leb, K. Kaproth-Joslin, and D. A. Lynch, "Practical Imaging Interpretation in Patients Suspected of Having Idiopathic Pulmonary Fibrosis: Official Recommendations from the Radiology Working Group of the Pulmonary Fibrosis Foundation," *Radiol. Cardiothorac. Imaging*, vol. 3, no. 1, p. e200279, Feb. 2021, doi: 10.1148/ryct.2021200279.

[28] D. A. Lynch *et al.*, "Diagnostic criteria for idiopathic pulmonary fibrosis: a Fleischner Society White Paper," *Lancet Respir. Med.*, vol. 6, no. 2, pp. 138–153, Feb. 2018, doi: 10.1016/S2213-2600(17)30433-2.

[29] M. Alsumrain *et al.*, "Combined pulmonary fibrosis and emphysema as a clinicoradiologic entity: Characterization of presenting lung fibrosis and implications for survival," *Respir. Med.*, vol. 146, pp. 106–112, Jan. 2019, doi: 10.1016/j.rmed.2018.12.003.

[30] "Nonspecific Interstitial Pneumonia - Pulmonary Disorders," *MSD Manual Professional Edition*. https://www.msdmanuals.com/professional/pulmonary-disorders/interstitial-lung-diseases/nonspecific-interstitial-pneumonia (accessed Feb. 13, 2022).

[31] T. Tateishi *et al.*, "Serial high-resolution computed tomography findings of acute and chronic hypersensitivity pneumonitis induced by avian antigen," *J. Comput. Assist. Tomogr.*, vol. 35, no. 2, pp. 272–279, Apr. 2011, doi: 10.1097/RCT.0b013e318209c5a6.

[32] M. Selman, "Hypersensitivity pneumonitis: a multifaceted deceiving disorder," *Clin. Chest Med.*, vol. 25, no. 3, pp. 531–547, vi, Sep. 2004, doi: 10.1016/j.ccm.2004.04.001.

[33] M. Silva, H. Nunes, D. Valeyre, and N. Sverzellati, "Imaging of Sarcoidosis," *Clin. Rev. Allergy Immunol.*, vol. 49, no. 1, pp. 45–53, Aug. 2015, doi: 10.1007/s12016-015-8478-7.

[34] E. Dhamija, "Cryptogenic organizing pneumonia | Radiology Reference Article | Radiopaedia.org," *Radiopaedia*. https://radiopaedia.org/articles/cryptogenic-organising-pneumonia-1 (accessed Jul. 01, 2022).

[35] M. Baque-Juston, A. Pellegrin, S. Leroy, C. H. Marquette, and B. Padovani, "Organizing pneumonia: What is it? A conceptual approach and pictorial review," *Diagn. Interv. Imaging*, vol. 95, no. 9, Art. no. 9, Sep. 2014, doi: 10.1016/j.diii.2014.01.004.

[36] "Signs and Patterns of Lung Disease - Chest Radiology: The Essentials, 2nd Edition." https://doctorlib.info/medical/chest/2.html (accessed Feb. 06, 2022).

[37] "The Radiology Assistant : Basic Interpretation." https://radiologyassistant.nl/chest/hrct/basic-interpretation (accessed Feb. 06, 2022).

[38] L. Li *et al.*, "Using Artificial Intelligence to Detect COVID-19 and Community-acquired Pneumonia Based on Pulmonary CT: Evaluation of the Diagnostic Accuracy," *Radiology*, vol. 296, no. 2, pp. E65–E71, Aug. 2020, doi: 10.1148/radiol.2020200905.

[39] M. P. Belfiore *et al.*, "Artificial intelligence to codify lung CT in Covid-19 patients," *Radiol. Med. (Torino)*, vol. 125, no. 5, pp. 500–504, May 2020, doi: 10.1007/s11547-020-01195-x.

[40] R. Grassi *et al.*, "COVID-19 pneumonia: computer-aided quantification of healthy lung parenchyma, emphysema, ground glass and consolidation on chest computed tomography (CT)," *Radiol. Med. (Torino)*, vol. 126, no. 4, pp. 553–560, Apr. 2021, doi: 10.1007/s11547-020-01305-9.

[41] M. Takahashi *et al.*, "Imaging of pulmonary emphysema: A pictorial review," *Int. J. Chron. Obstruct. Pulmon. Dis.*, vol. 3, no. 2, pp. 193–204, Jun. 2008.

[42] D. C. Caltabiano *et al.*, "Cystic pattern in lung diseases: a simplified HRCT guide based on free-hand drawings," *ECR 2017 EPOS*, Mar. 01, 2017. https://epos.myesr.org/poster/esr/ecr2017/C-2141 (accessed Feb. 13, 2022).

[43] "Fleischner Society: Glossary of Terms for Thoracic Imaging | Radiology." https://pubs.rsna.org/doi/abs/10.1148/radiol.2462070712?journalCode=radiology (accessed Feb. 06, 2022).

[44] Collins Jannette and Stern Eric J, "Alveolar Lung Disease - Chest Radiology: The Essentials, 2nd Edition." https://doctorlib.info/medical/chest/4.html (accessed Feb. 06, 2022).

[45] P. P. T. E. S. Torres, M. F. Rabahi, M. A. do C. Moreira, D. L. Escuissato, G. de S. P. Meirelles, and E. Marchiori, "Importance of chest HRCT in the diagnostic evaluation of fibrosing interstitial lung diseases," *J. Bras. Pneumol. Publicacao Of. Soc. Bras. Pneumol. E Tisilogia*, vol. 47, no. 3, p. e20200096, 2021, doi: 10.36416/1806-3756/e20200096.

[46] G. Dalpiaz and A. Cancellieri, "Alveolar Pattern," *Atlas Diffuse Lung Dis.*, pp. 145–162, Dec. 2016, doi: 10.1007/978-3-319-42752-2_9.

[47] C. A. Ridge, A. A. Bankier, and R. L. Eisenberg, "Mosaic attenuation," *AJR Am. J. Roentgenol.*, vol. 197, no. 6, pp. W970-977, Dec. 2011, doi: 10.2214/AJR.11.7067.

[48] F. Gaillard, "Head cheese sign (lungs) | Radiology Reference Article | Radiopaedia.org," *Radiopaedia*. https://radiopaedia.org/articles/head-cheese-sign-lungs (accessed Feb. 12, 2022).

[49] S. E. Rossi, J. J. Erasmus, M. Volpacchio, T. Franquet, T. Castiglioni, and H. P. McAdams, "'Crazy-Paving' Pattern at Thin-Section CT of the Lungs: Radiologic-Pathologic Overview," *RadioGraphics*, vol. 23, no. 6, pp. 1509–1519, Nov. 2003, doi: 10.1148/rg.236035101.

[50] N. Gupta, R. Vassallo, K. A. Wikenheiser-Brokamp, and F. X. McCormack, "Diffuse Cystic Lung Disease. Part II," *Am. J. Respir. Crit. Care Med.*, vol. 192, no. 1, pp. 17–29, Jul. 2015, doi: 10.1164/rccm.201411-2096CI.

[51] S. R. Desai, H. Prosch, and J. R. Galvin, "Plain Film and HRCT Diagnosis of Interstitial Lung Disease," in *Diseases of the Chest, Breast, Heart and Vessels 2019-2022: Diagnostic and Interventional Imaging*, J. Hodler, R. A. Kubik-Huch, and G. K. von Schulthess, Eds. Cham (CH): Springer, 2019. Accessed: Feb. 06, 2022. [Online]. Available: http://www.ncbi.nlm.nih.gov/books/NBK553872/

[52] G. V. L. de Lima, T. R. Castilho, P. H. Bugatti, P. T. M. Saito, and F. M. Lopes, "A Complex Network-Based Approach to the Analysis and Classification of Images," in *Progress in Pattern Recognition, Image Analysis, Computer Vision, and Applications*, Cham, 2015, pp. 322–330. doi: 10.1007/978-3-319-25751-8_39.

[53] G. Veloso, T. Castilho, P. Bugatti, P. Saito, and F. Lopes, *A Complex Network-Based Approach to the Analysis and Classification of Images*. 2015. doi: 10.1007/978-3-319-25751-8_39.

[54] Y. Mourchid, M. E. Hassouni, and H. Cherifi, "A General Framework for Complex Network-Based Image Segmentation," *Multimed. Tools Appl.*, vol. 78, no. 14, pp. 20191–20216, Jul. 2019, doi: 10.1007/s11042-019-7304-2.

[55] L. da F. Costa, F. A. Rodrigues, G. Travieso, and P. R. Villas Boas, "Characterization of complex networks: A survey of measurements," *Adv. Phys.*, vol. 56, no. 1, pp. 167–242, Jan. 2007, doi: 10.1080/00018730601170527.

[56] A. M. Nambiar, C. M. Walker, and J. A. Sparks, "Monitoring and management of fibrosing interstitial lung diseases: a narrative review for practicing clinicians," *Ther. Adv. Respir. Dis.*, vol. 15, p. 17534666211039772, Sep. 2021, doi: 10.1177/17534666211039771.

 doi:10.20944/preprints202208.0099.v1

Abbreviation List

AIP- acute interstitial pneumonia
CAD- Computer Aided Diagnosis
CN-Complex Networks
CPFE-combined pulmonary fibrosis and emphysema
CT-Computer Tomography
DILD- Diffuse interstitial lung diseases
DIP-desquamative interstitial pneumonia,
DILD- diffuse interstitial lung diseases
Dlco- diffusing capacity of the lungs for carbon monoxide
FVC- forced vital capacity
GE- General Electrics
GGO- Ground Glass Opacity
HRCT-High Resolution Computed Tomography
HPc-Chronic Hypersensitivity Pneumonitis
HU-Hounsfield Unit
ILD-Interstitial Lung Diseases
IPF-Idiopathic Pulmonary Fibrosis
LAM-lymphangiomyomatosis
LCH-Langerhans cell histiocytosis
LIP-lymphoid interstitial pneumonia
NSIP-Non-Specific Interstitial Pneumonia
MDD-Multidisciplinary discussion
OP- Organizing Pneumonitis
PAP-Pulmonary Alveolar Proteinosis
PCR- Polymerase Chain Reaction
PFT- Pulmonary Function Test
PF-ILD- progressive fibrosing interstitial lung disease
PPFE-pleuroparenchymal fibroelastosis
RB-ILD -respiratory bronchiolitis-associated interstitial lung disease
S-Sarcoidosis
SPL- Secondary Pulmonary Lobule
UIP- Usual Interstitial Pneumonia